ADVANCED FUNCTIONAL MATERIALS

Supporting Information

Localized Laser-Based Photohydrothermal Synthesis of Functionalized Metal-Oxides

Kyungmook Kwon, Jaeho Shim, Jeong Oen Lee, Kyunghan Choi, and Kyoungsik Yu*

Supporting Information

Localized laser-based photohydrothermal synthesis of functionalized metal-oxides

Kyungmook Kwon, Jaeho Shim, Jeong Oen Lee, Kyunghan Choi, Kyoungsik Yu[*]

 [*] Corresponding author: Prof. Kyoungsik Yu

Department of Electrical Engineering, KAIST

Daejeon, 305-701, South Korea

E-mail: ksyu@kaist.edu

(a)

| Initial stage | Continuous heating | Continuous heating |

(b)

| Initial stage | Heating cycle | Cooling cycle |
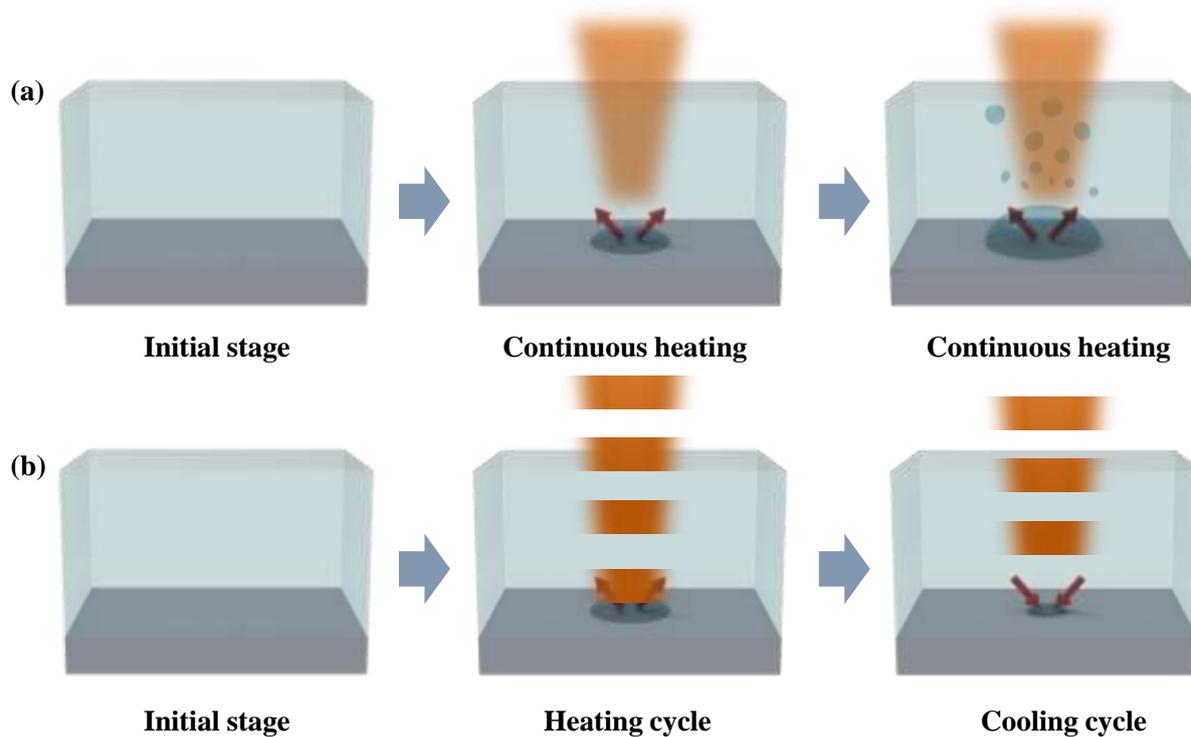
Figure S1. In the conventional large-area bulk heating, it is hard to exceed the boiling point under the normal ambient pressure. However, PLIH can easily achieve the superheating condition while preventing explosive bubble generation. (a) Under continuous heating, the vapor layer continuously grows up, and the excessive vapor pressure results in explosive bubble generation. (b) With PLIH, the vapor layer collapses during the cooling cycle.
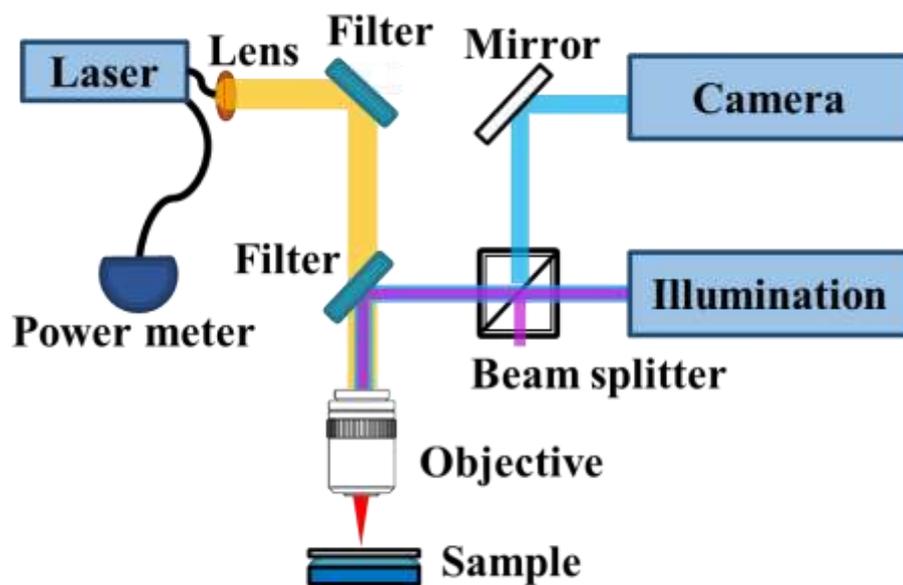
Figure S2. A schematic diagram of the experimental setup for the localized photohydrothermal synthesis of metal oxide materials with focused laser beam irradiation.
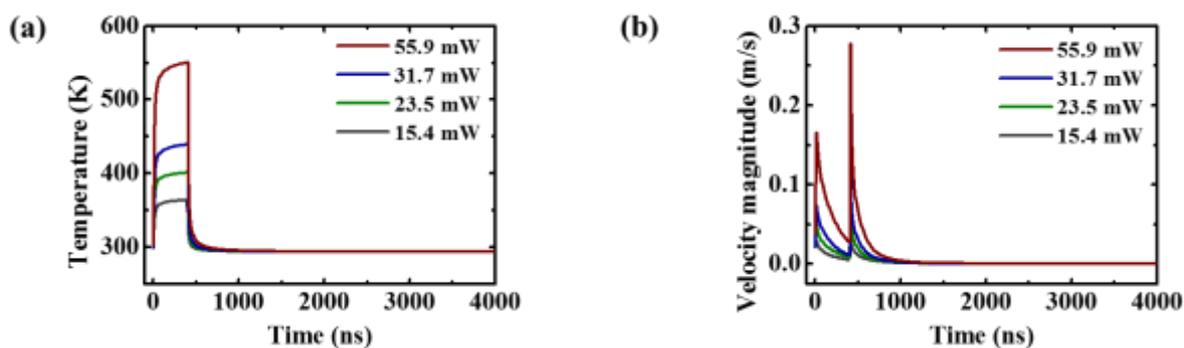
Figure S3. (a) Temperature variation from the periodic heating and cooling cycles of PLIH with various laser peak powers on the 40-nm-thick tungsten film. A heating (illumination) period of 400 ns and cooling period of 3600 ns (10% duty cycle) were chosen to minimize thermal diffusion and complete cooling between the optical pulses. The peak temperature rises above the atmospheric boiling point when the incident laser peak power becomes large enough (>23.5 mW). (b) Time evolution of peak flow velocity with respect to various laser peak powers for PLIH. Fast fluid flow velocities result from the steep temperature gradient produced by rapid switching of laser illumination. PLIH provides the efficient mass transport of precursor, exhibiting a local maximum fluid velocity of ~6 cm/s with a 23.5 mW peak power. The results are obtained by finite element method simulations.
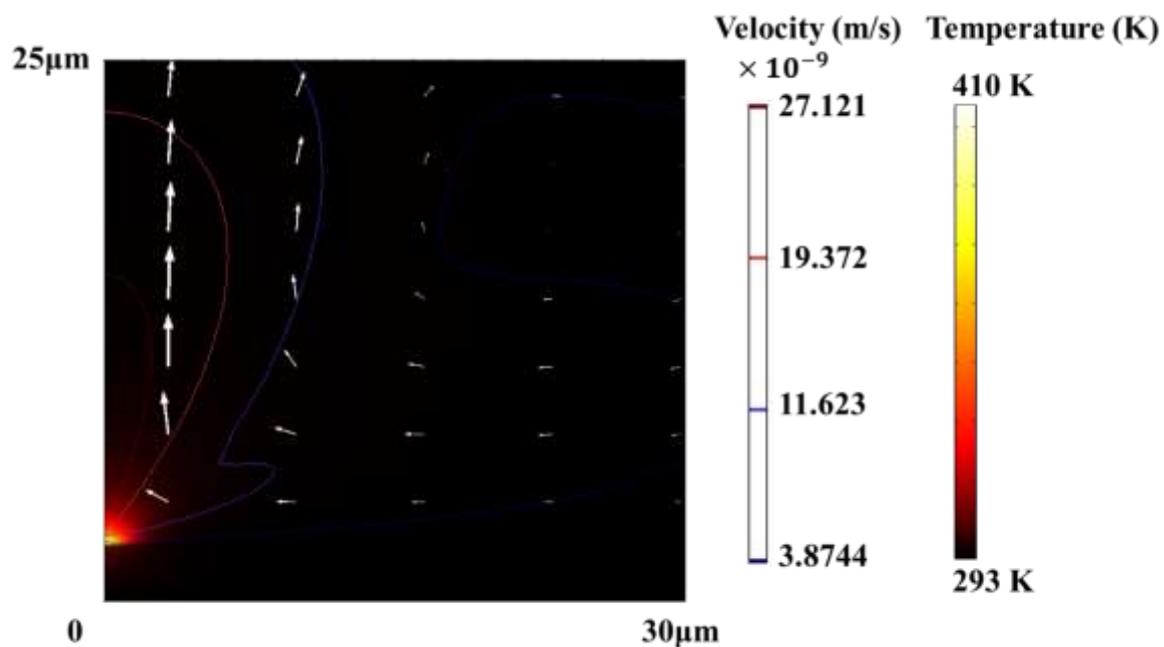
Figure S4. Flow velocity profile at 10 seconds with continuous-wave laser illumination (23.5 mW). Under the continuous laser irradiation, the fluid velocity is below 1 μm/s which is quite slow compared to PLIH in Figure S3. The result is obtained by finite element method simulations.
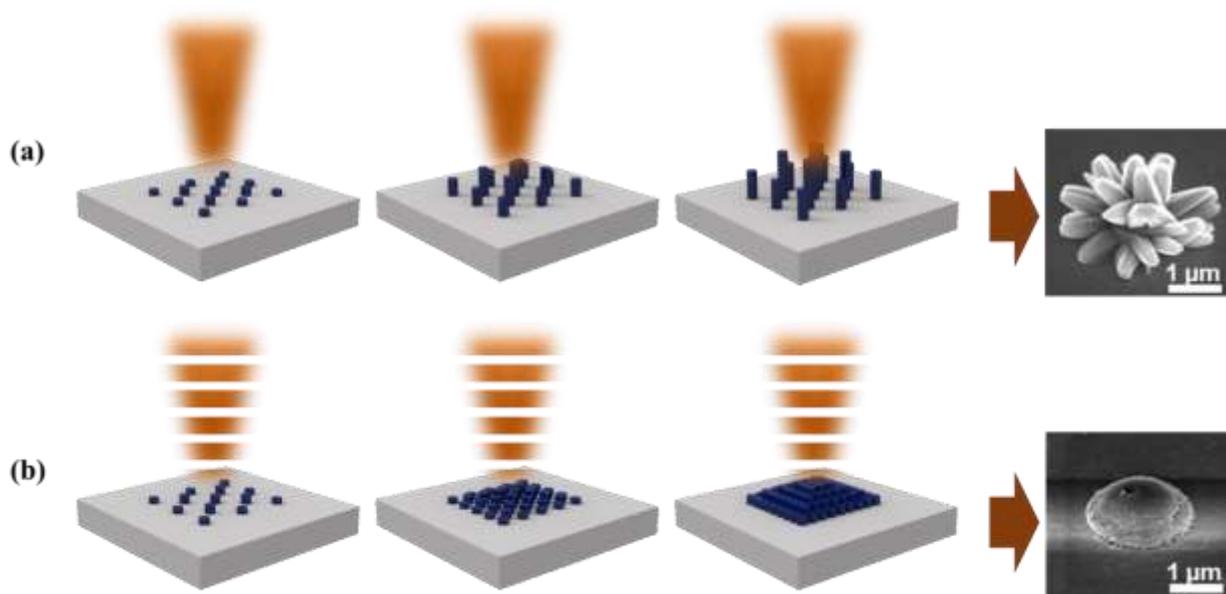
Figure S5. Schematic illustration of the growth mechanism for the conventional continuous-heated hydrothermal method (a) and the proposed PLIH-based technique (b). (a) Under the continuous-heated hydrothermal method, metal-oxides synthesis follows the crystalline of the existing structures and forms nanowires. (b) In the proposed photohydrothermal method with PLIH, thermal energy is highly confined only near the metal absorption layer due to the repeated heating and cooling cycles without much thermal diffusion. Furthermore, synthesis temperature during the laser illumination is relatively high, and crystal nucleation is therefore a dominant process. Therefore, metal oxide materials are synthesized from the metal absorption layer, and as a result highly-packed metal-oxides bumps can be obtained.
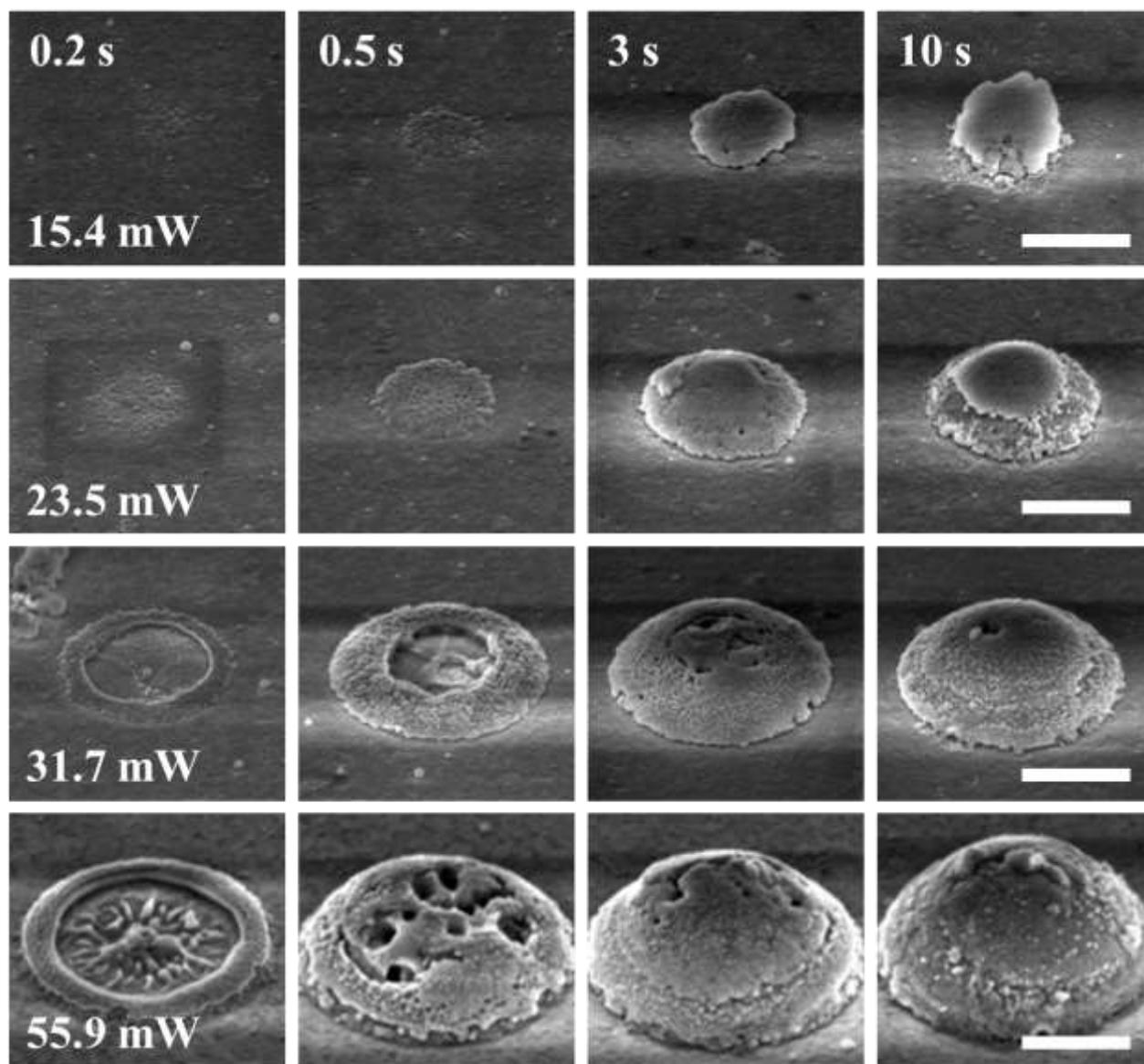
Figure S6. SEM images of zinc oxide bumps photohydrothermally grown on a tungsten film with various laser peak powers (15.4, 23.5, 31.7, and 55.9 mW) and growth times (0.2, 0.5, 3, and 10 seconds). All scale bars represent 1 μm.
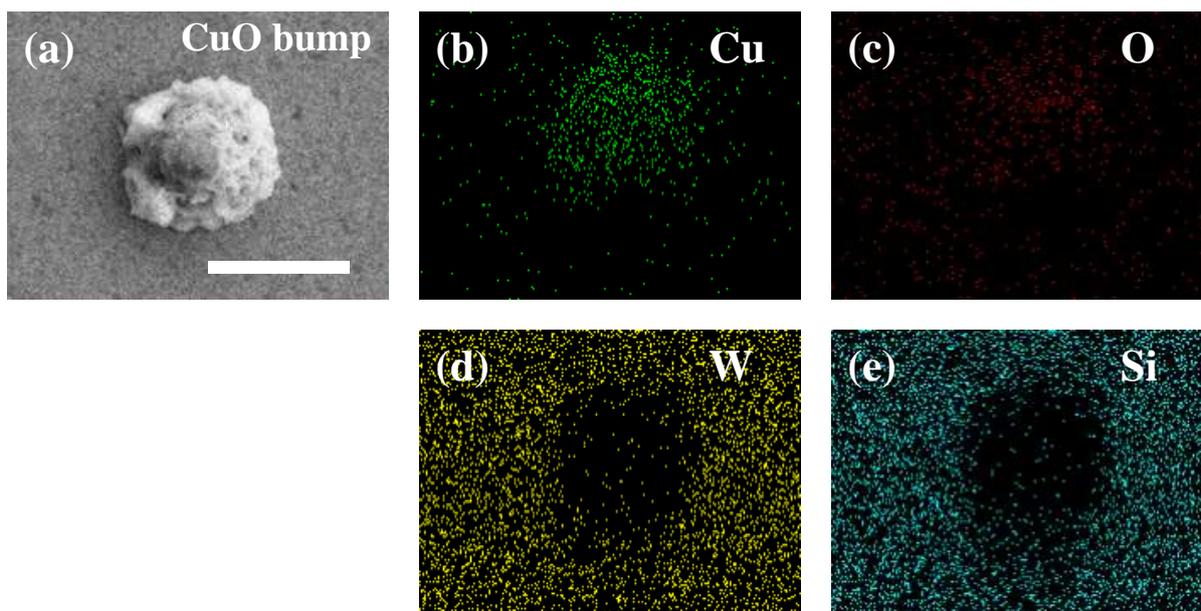
Figure S7. (a) SEM image of a CuO bump and (b-e) the corresponding EDS elemental mappings show the spatial distribution of Cu (green), O (red), W (yellow) and Si (blue), respectively. The distribution of Cu and O confirms that the synthesized bump contains both Cu and O. The elements observed outside the bump region (O, W, Si) mainly come from the substrate (Si/SiO$_2$/W). A 10 kV beam energy was used for EDS, and the scale bar represents 2 μm.

(a)

(b)
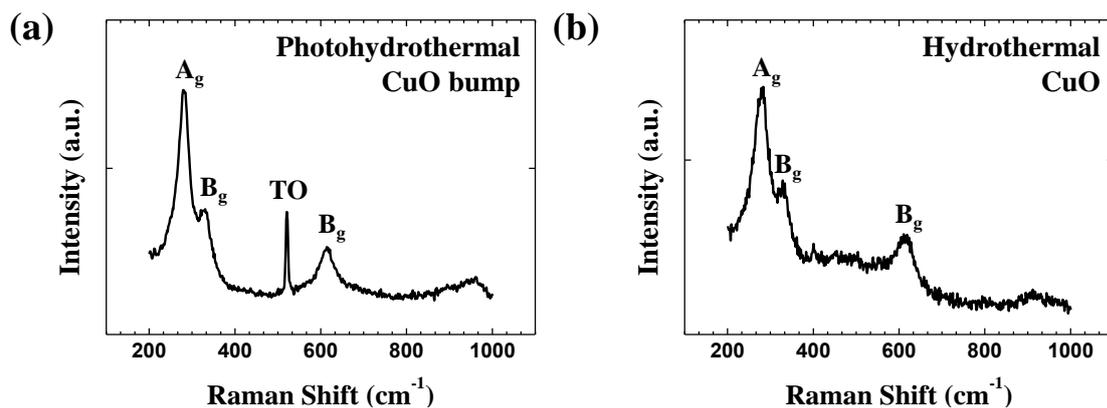
Figure S8. Raman spectra of (a) a photohydrothermally-grown CuO bump on the Si/SiO$_2$/W substrate, and (b) a hydrothermally-synthesized CuO material on the glass substrate. From the Raman spectrum of a CuO bump in (a), both the A$_g$ (~280 cm^{-1}) and B$_g$ mode (~330 cm^{-1} and ~615 cm^{-1}) indicate that the synthesized material is actually CuO.[1] This result is equivalent to the Raman spectrum of a hydrothermally synthesized CuO material shown in (b). The TO peak at ~520 cm^{-1} in (a) is from the silicon substrate.[2] A 514 nm laser was used as an exitation light source for Raman measurements.
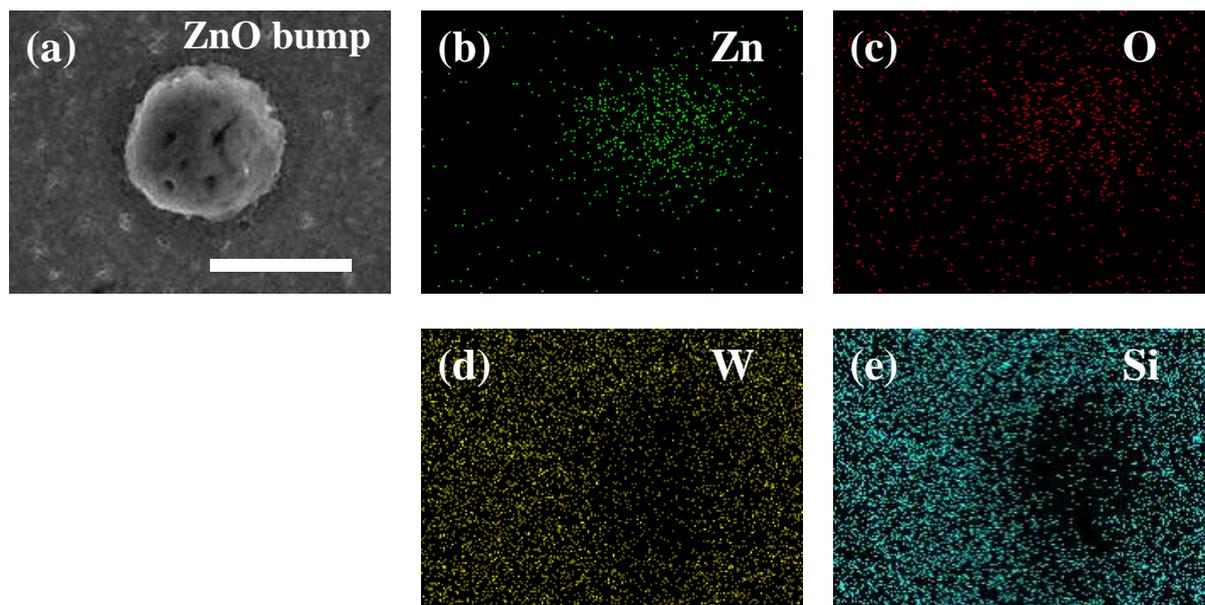
Figure S9. (a) SEM image of a ZnO bump and (b-e) the corresponding EDS elemental mappings show the spatial distribution of Zn (green), O (red), W (yellow) and Si (blue). The spatial distribution of Zn and O represents that the synthesized bump contains both Zn and O. A 10 kV beam energy was used for EDS, and the scale bar represents 2 μm.

WILEY-VCH
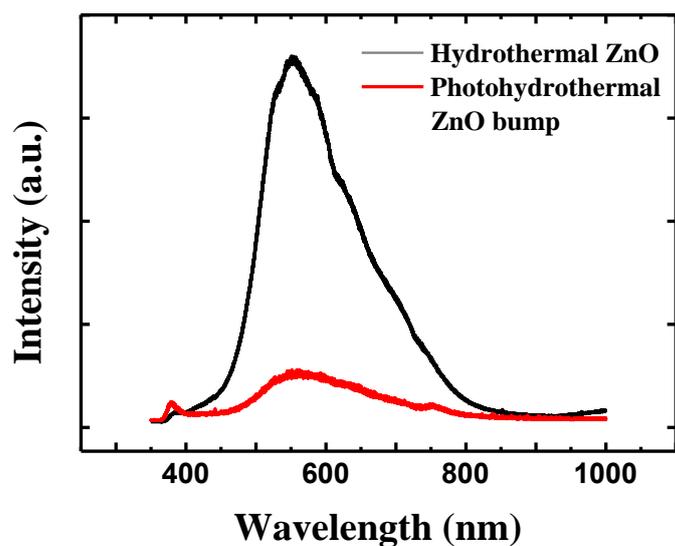
Figure S10. The photoluminescence from a photohydrothermal ZnO bump and a hydrothermal ZnO material. Discrepancies in the emission spectra are believed to be originated from the different density of defects, such as interstitial oxygen, oxygen vacancies, interstitial zinc, and zinc vacancies. The relative density distributions of such defects are related with the morphologies of the synthesized ZnO material.[3] It is interesting to note that we were able to observe strong band edge emission from a photohydrothermally-grown ZnO bump with ultra-short synthesis time.
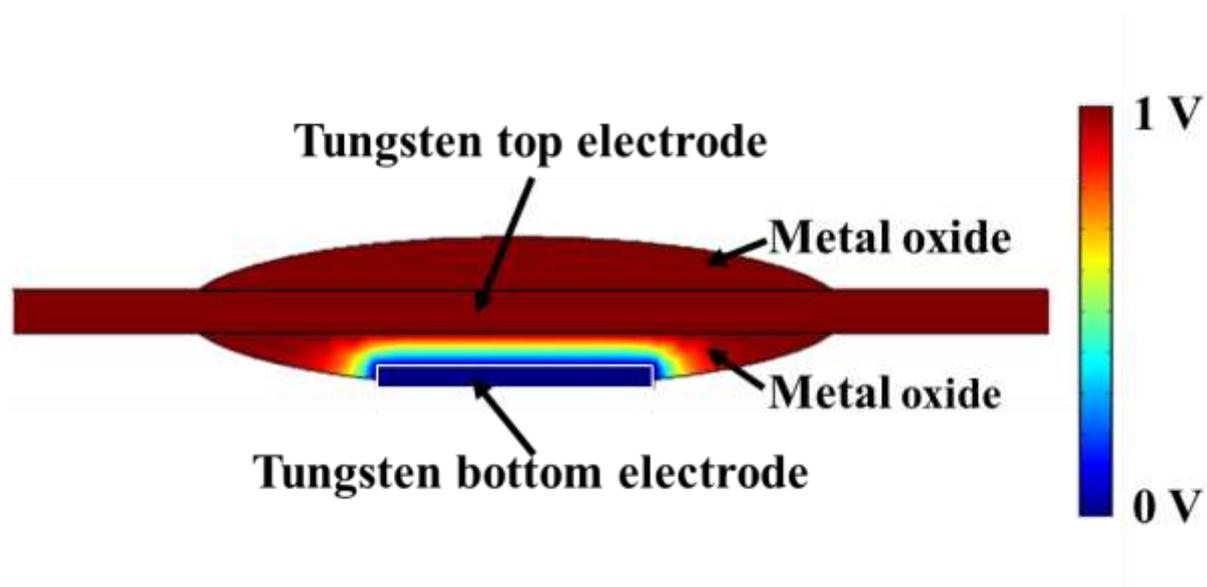
Figure S11. Voltage distribution profile when 1 V is applied between the top and bottom tungsten metal strip. The voltage drop mainly occurs at the metal oxide material sandwiched between the top and bottom electrode.
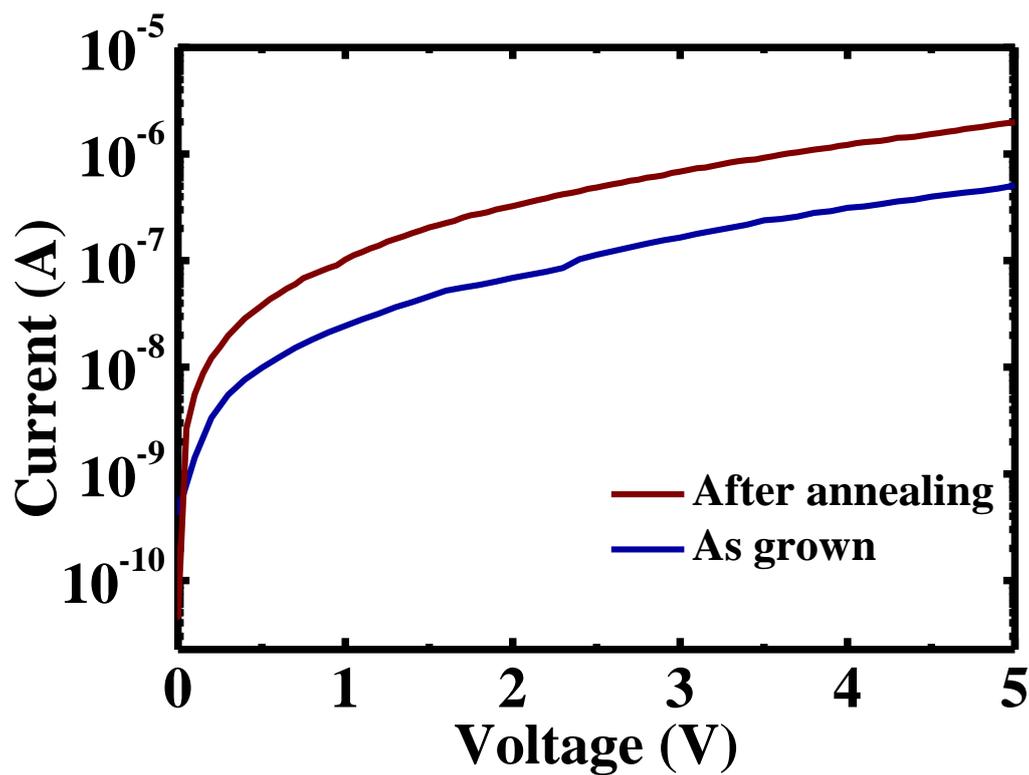
Figure S12. To demonstrate the effect of an additional annealing process, the metal strip lines electrically connected by a zinc oxide bump was annealed at 260 ℃ for ten hours in the nitrogen atmosphere. After the annealing process, the conductivity of the zinc oxide solder bump was significantly enhanced.

Reference for Supporting Information

[1]   W. Wang, Q. Zhou, X. Fei, Y. He, P. Zhang, G. Zhang, L. Peng, W. Xie, Crystengcomm **2010**, 12, 2232.
[2]   E. Quiroga-Gonzalez, J. Carstensen, C. Glynn, C. O'Dwyer, H. Foell, Physical Chemistry Chemical Physics **2014**, 16, 255.
[3]   T.-J. Liu, Q. Wang, P. Jiang, Rsc Advances **2013**, 3, 12662; A. B. Djurisic, Y. H. Leung, Small **2006**, 2, 944.